

Phase Space Reconstruction from Accelerator Beam Measurements Using Neural Networks and Differentiable Simulations

R. Roussel,* A. Edelen, C. Mayes, and D. Ratner
SLAC National Accelerator Laboratory, Menlo Park, CA 94025, USA

J.P. Gonzalez-Aguilera
University of Chicago, Chicago, Illinois 60637, USA

S. Kim, E. Wisniewski, J. Power
Argonne National Laboratory, Argonne, Illinois 60439, USA
(Dated: September 13, 2022)

Characterizing the phase space distribution of particle beams in accelerators is a central part of accelerator understanding and performance optimization. However, conventional reconstruction-based techniques either use simplifying assumptions or require specialized diagnostics to infer high-dimensional ($> 2D$) beam properties. In this Letter, we introduce a general-purpose algorithm that combines neural networks with differentiable particle tracking to efficiently reconstruct high-dimensional phase space distributions without using specialized beam diagnostics or beam manipulations. We demonstrate that our algorithm reconstructs detailed 4D phase space distributions with corresponding confidence intervals in both simulation and experiment using a single focusing quadrupole and diagnostic screen. This technique allows for the measurement of multiple correlated phase spaces simultaneously, enabling simplified 6D phase space reconstruction diagnostics in the future.

Increasingly precise control of the distribution of particles in position-momentum phase space is needed for emerging applications of accelerators [1]. This includes, for example, new experiments at free electron lasers [2–6] and novel acceleration schemes that promise higher-energy beams in compact spaces [7]. Numerous techniques have been developed for precision shaping of beam distributions (e.g. [8–10]); however, the effectiveness of these techniques relies on accurate measurements of the 6D phase space distribution, which is a challenging task unto itself.

Tomographic measurement techniques are used in accelerators to determine the density distribution of beam particles in phase space $\rho(x, p_x, y, p_y, z, p_z)$ from limited measurements [11–16]. The simplest example of this is commonly referred to as a quadrupole scan, where the strength of a quadrupole focusing magnet is varied while measuring the transverse (x, y) beam size at a downstream scintillating screen [17–19]. This process however, makes simplifying assumptions about the beam distribution, discarding rich information captured by diagnostic screens and ignoring realistic beam attributes.

In contrast, methods using projections of the beam image, including filtered back-projection [14, 20], algebraic reconstruction [21], and maximum entropy tomography (MENT) [15, 22] produce more accurate reconstructions. The MENT algorithm is particularly well-suited to reconstructing beams from limited and/or partial information sources about the beam distribution, as is the case in most experimental accelerator measurements. MENT

performs reconstruction by producing a beam distribution that maximizes entropy (and, as a result, likelihood), subject to the constraint that the distribution reproduces measurements accurately. While these methods have been shown to effectively reconstruct 2D phase spaces from image projections using algebraic methods, application to higher-dimensional spaces requires independence assumptions between the phase spaces of principal coordinate axes (x, y, z) , complicated phase space rotation procedures [23], or measurement of multiple 2D sub-spaces with specialized diagnostic hardware [24].

It is also possible to directly fit a beam distribution to experimental data by iteratively generating a large number of simulated particles on a mesh, based on a simple heuristic or optimization routine, until the set of particles produces correct results [25, 26]. This brute force method is computationally expensive to implement and does not account for the likelihood of the reconstructed distribution.

In this Letter we describe a new method that provides detailed reconstructions of the beam phase space using simple and widely-available accelerator elements and diagnostics. To achieve this, we take advantage of recent developments in machine learning to introduce two new concepts (shown in Fig. 1): a method for parameterizing arbitrary beam distributions in 6D phase space, and a differentiable particle tracking simulation that allows us to learn the beam distribution from arbitrary downstream accelerator measurements. We examine how this method extracts detailed phase space distributions from a tomographic beamline containing a single quadrupole, drift and diagnostic screen to image the transverse (x, y) distribution for both synthetic and experimental beam distributions. Finally, we discuss current limitations of

* roussel@slac.stanford.edu

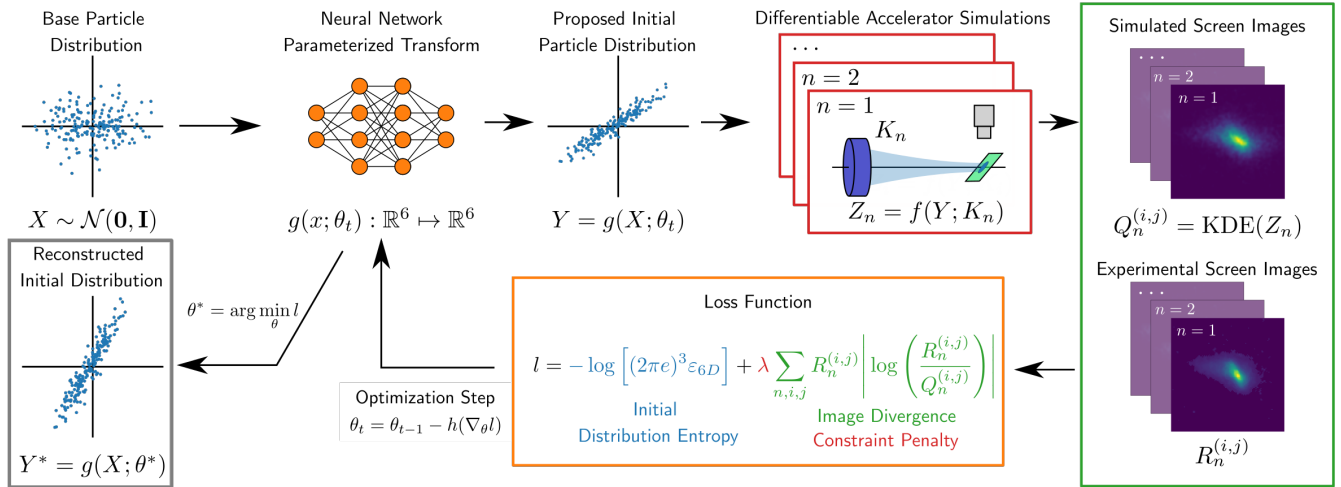


FIG. 1. Description of our approach for reconstructing 6D phase space beam distributions. First, a base distribution is transformed via neural network, parameterized by θ , into a proposed initial distribution. This distribution is then transported through a differentiable accelerator simulation of the tomographic beamline. The quadrupole is scanned to produce a series of images on the screen, both in simulation and on the operating accelerator. The images produced both from the simulation $Q_n^{(i,j)}$ and the accelerator $R_n^{(i,j)}$ are then compared with a custom loss function, which attempts to maximize the entropy of the proposal distribution, constrained on accurately reproducing experimental measurements. This loss function is then used to update the neural network parameters via gradient descent. The neural network transformation that minimizes the loss function, generates the beam distribution that has the highest likelihood of matching the real initial beam distribution.

this method as well as future directions for the design of novel accelerator diagnostics using this technique.

We first demonstrate our algorithm using a synthetic example, where we attempt to determine the distribution of a 10-MeV beam given a predefined structure in 6D phase space. Projections of the synthetic beam distribution in phase space at the entrance to a diagnostic lattice containing a 10 cm long quadrupole, 1.0 m long drift and a transverse screen are shown in Fig. 2(a-c). To illustrate the capabilities of our technique, the synthetic beam contains multiple higher order moments between each phase space coordinates (see Supplemental Materials for details). We generate simulated images resulting from 20 different quadrupole strengths k_n using a custom implementation of Bmad [27] referred to here as Bmad-X. Particles then travel through a drift to a simulated 200×200 pixel screen where each pixel has a transverse resolution of $300 \mu\text{m}$. The set of images, where the intensity of pixel (i, j) on the n 'th image is represented by $R_n^{(i,j)}$, are then collected with the corresponding quadrupole strengths to create the data set, which is then split into training and testing subsets by selecting every other sample as a test sample, resulting in 10 samples for each data subset.

The reconstruction algorithm begins with the generation of arbitrary initial beam distributions (referred to here as proposal distributions) through the use of a neural network transformation. A neural network is used to transform samples drawn from a 6D normal distribution centered at the origin to macro-particle coordinates in real 6D phase space (where positional coordinates are

given in meters, momentum coordinates are in radians for transverse momenta). The network itself is relatively small, consisting of only 4 fully-connected layers of 50 neurons each to minimize training time while maintaining transformation complexity (see Supplemental Materials for details).

Fitting neural network parameters to experimental measurements is done by minimizing a loss function to determine the most likely initial beam distribution, subject to the constraint that it reproduces experimental measurements, similar to the MENT algorithm [22]. The likelihood of an initial beam distribution in phase space is maximized by maximizing the distribution entropy, which is proportional to the log of the 6D beam emittance ϵ_{6D} [28]. Thus, we specify a loss function that minimizes the negative entropy of the proposal beam distribution, penalized by the degree to which the proposal distribution reproduces measurements of the transverse beam distribution at the screen location. To evaluate the penalty for a given proposal distribution, we track the proposal distribution through a batch of accelerator simulations that mimic experimental conditions to generate a set of simulated images $Q_n^{(i,j)}$ to compare with experimental measurements. The total loss function is given by

$$l = -\log \left[(2\pi e)^3 \epsilon_{6D} \right] + \lambda \sum_{n,i,j} R_n^{(i,j)} \left| \log \left(\frac{R_n^{(i,j)}}{Q_n^{(i,j)}} \right) \right| \quad (1)$$

where λ scales the constraining penalty function (in this work we specify $\lambda = 10^3$).

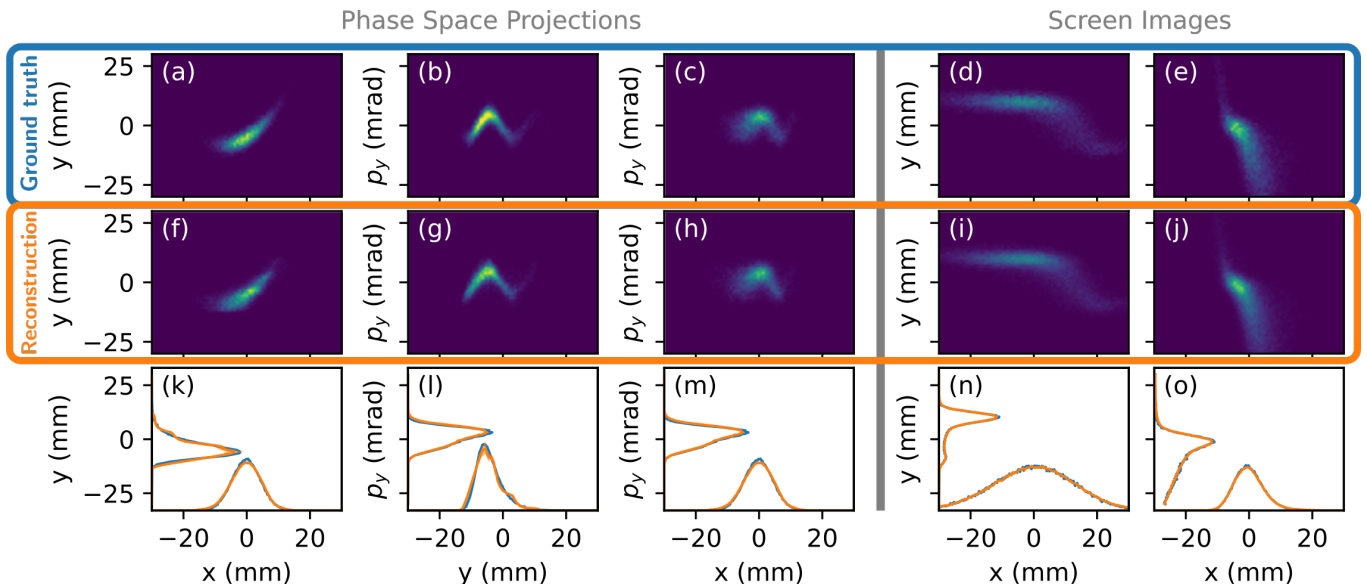


FIG. 2. Comparisons between the synthetic and reconstructed beam probability distributions using our method. A synthetic beam with a tailored phase space distribution (a-c) is transported through a diagnostic beamline with varying quadrupole strengths, producing 10 training images and 10 test images which are not included in model training, 2 of which are shown in (d-e). Using the training images, our algorithm predicts the phase space distribution (for which a subset of projections is shown in f-h) and screen images corresponding to the test set (i-j). Comparison between ground truth and reconstructed 1D projections for corresponding 2D plots are shown in (k-o).

However, the large ($> 10^4$) number of free parameters contained in the neural network transformation used to generate proposal distributions necessitates the use of gradient-based optimization algorithms such as Adam [29] to minimize the loss function. Thus, we need a loss function that is *differentiable* [30], i.e. we need to be able to analytically compute the derivative of the loss function with respect to every neural network parameter. This requires that every step involved in calculating the loss function is also differentiable, including calculating the beam emittance and tracking particles through the accelerator. Unfortunately, no particle tracking codes which are differentiable with respect to particle coordinates currently exist. To satisfy this requirement, we implement particle tracking using Bmad-X combined with the differentiable machine learning library *PyTorch* [31]. We also replace histograms used to simulate screen pixel intensities with a differentiable implementation of kernel density estimation [32].

Results from our reconstruction of the initial beam phase space using synthetic images are shown in Fig. 2. We see excellent agreement between the average reconstructed and synthetic projections in both transverse correlated and uncorrelated phase spaces. Furthermore, we are able to accurately predict screen images excluded from the training set. Numerical predictions of the 2D transverse phase space normalized emittances ($\varepsilon_{x,n} = 2.19 \pm 0.07$ mm-mrad, $\varepsilon_{y,n} = 17.10 \pm 0.34$ mm-mrad) closely matches the true synthetic beam emittances ($\varepsilon_{x,n} = 2.00$ mm-mrad, $\varepsilon_{y,n} = 15.60$ mm-mrad).

We characterize the confidence of our reconstruction using snapshot ensembling [33]. During model training we cycle the learning rate of gradient descent in a periodic fashion, saving model parameters at the minima of the learning rate cycle, as shown in Fig. 3(a). This encourages the optimizer to explore multiple possible solutions (if they exist). We then use equal weighting between models to make a mean prediction of the initial beam distribution with associated confidence intervals.

As a result, it is instructive to examine the evolution of the proposal distribution during model training. In Fig. 3(b-c) we examine scalar metrics of the proposal distribution after each training iteration, including the principal phase space emittances and the beamsizes in each phase space coordinate. The phase space components that have the strongest impact on beam transport through the beamline as a function of quadrupole strength converge quickly, whereas the ones that have little-to-no impact (e.g. the longitudinal distribution characteristics) do not. Results shown in Fig. 3(b-c) are consistent with expectations given the beamline elements as transport is independent of the longitudinal beam distribution. In particular, we observe that each snapshot converges to beam distributions which have slightly varying energy spreads, signifying uncertainty in that aspect of the beam's phase space, likely due to weak coupling between energy spread and transverse beam size through chromatic aberrations in the quadrupole. The convergence of the proposal distribution thus provides a useful indicator of which components of the phase space can be reliably reconstructed for arbitrary (possibly unknown)

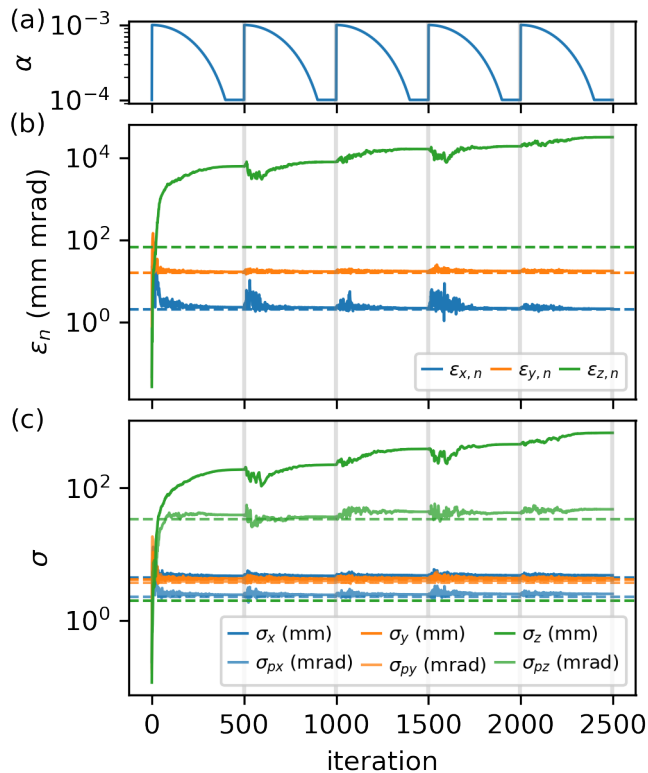


FIG. 3. Evolution of the proposal distribution during training on synthetic data. (a) Learning rate schedule for snapshot ensembling. (b) Two dimensional beam emittances along principal beam axes (x, y, z). (c) Root mean squared beam sizes for each phase space coordinate. Dotted lines denote ground truth values. Vertical lines denote snapshot locations.

tomographic beamlines.

We now describe a demonstration of our method on an experimental example at the Argonne Wakefield Accelerator (AWA) [34] facility at Argonne National Laboratory. Here we are interested in determining the phase space distribution of 65-MeV electron beams at the exit of the main drive beamline. The focusing strength a quadrupole, with an effective length of 12 cm, is scanned while imaging the beam at a transverse scintillating screen 3.38 m downstream. Charge windowing, image filtering, thresholding and downsampling were used to generate a set of 3 images for each quadrupole setting (see Supplemental Materials for additional details).

We then created a simulation in Bmad-X of the experimental beamline, including the details of the diagnostics used (e.g. the location properties of beamline elements and per-pixel resolution of the imaging screen). This was then used to reconstruct the initial beam distribution using our reconstruction method. Results from the reconstruction are shown in Fig. 4. We observe that the reconstruction is able to resolve the minor features contained in the training images. Since we are able to accurately predict the overall beam size and minor features in the test images (see Supplemental Materials for detailed

images), we conclude that the reconstructed initial beam distribution should closely match the real beam distribution. Projections of the reconstructed beam distribution are shown in Fig. 4(b-g), where we observe weak mixing between the two transverse phase spaces, which possibly result from non-ideal fields in the AWA photoinjector [35]. Further, the emittance of the reconstructed beam along both transverse axes ($\varepsilon_{x,n} = 14.90 \pm 0.03$ mm-mrad, $\varepsilon_{y,n} = 14.00 \pm 0.01$ mm-mrad) shows reasonable agreement with beam emittances calculated from scalar beam size measurements ($\varepsilon_{x,n} = 22.17 \pm 0.27$ mm-mrad, $\varepsilon_{y,n} = 12.14 \pm 0.93$ mm-mrad).

The disagreement between these two methods might have multiple sources. First, the calculation of beam emittance from scalar beam size values assumes a perfectly Gaussian beam. We can clearly see from our measurements that the beam is not Gaussian, resulting in potential emittance calculation errors. Second, our simulation does not contain fringe fields inside the quadrupole, which are likely present in the real magnet, thus leading to reconstruction errors, especially for higher quadrupole strengths as observed in Fig. 4(a). Incorporating more accurate simulations into our reconstruction procedure should improve the reconstruction accuracy.

In this work we have demonstrated how machine learning techniques, namely the parameterization of beam distributions in 6D phase space using neural networks, combined with differentiable particle tracking, can be used to create detailed reconstructions of the phase space distribution. We demonstrated that our technique is able to generate detailed 4D phase space reconstructions in both simulation and experiment, using a single quadrupole scan and diagnostic screen. Our approach eliminates the need for beam approximations, specialized diagnostics, or complicated tomographic beam manipulations to reconstruct the high dimensional phase space structure of the beam distribution.

In contrast to currently-used beam diagnostics, which isolate individual components of the beam distribution, our method enables the simultaneous combination of multiple measurement techniques to reconstruct the beam distribution in higher-dimensional phase spaces, accounting for nuanced correlations between subspaces. As a result, combinations of diagnostic techniques can be used simultaneously to resolve larger portions of the phase space distribution, exactly or partially. For example, the addition of a transverse deflecting cavity and a dipole spectrometer to the diagnostic beamline examined here will enable accurate 6D phase space reconstructions using simple transverse imaging of the beam with a limited number of measurements.

The use of differentiable physics simulations is what enables the flexibility and fidelity of our reconstruction technique. Differentiable physics simulations allows us to perform high-dimensional parameter estimation unbounded by analytical tractability. As a result, our analysis is limited only by the accuracy and computational cost of the physics simulations themselves. In the future,

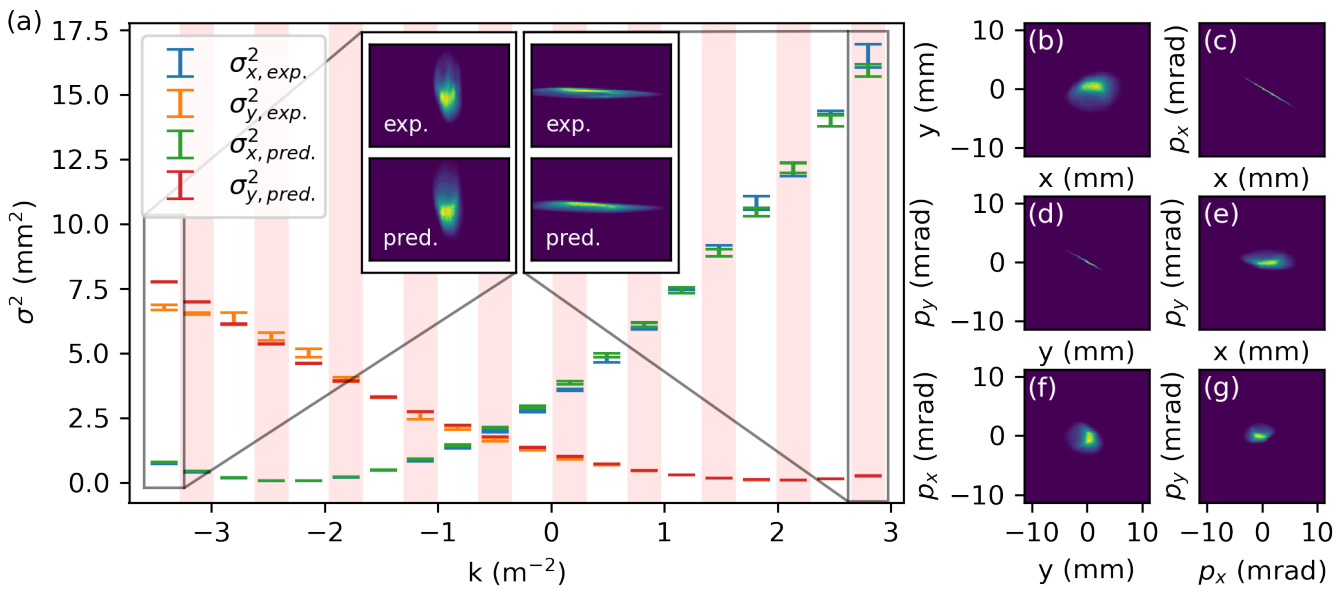


FIG. 4. Reconstruction results from experimental measurements at AWA. (a) Measurements of RMS beam size squared (σ^2) as a function of geometric quadrupole focusing strength (k) using experimental and predicted images. Inset: Comparison between real and predicted screen images. Red shading denotes test samples not used to train the reconstruction. (b-g) Average phase space distributions of reconstructed beams from snapshot ensemble.

our analysis could include differentiable simulations of nonlinear collective effects such as coherent synchrotron radiation [36], wakefields and particle-particle interactions like space charge [37]. This opens up new possibilities for accelerator diagnostics beyond what is normally used in the field today, for example, diagnosing longitudinal bunch profiles using wakefield effects [38]. Furthermore, the need to perform high-dimensional parameter estimation in accelerators is not unique to the reconstruction of beam distributions. For example, in our previous work, we determined detailed hysteresis properties of magnetic accelerator elements using a differentiable physics model [39].

As with any new algorithmic technique, there are several areas for future improvement that we now plan to address in order to make the algorithm fully practical for routine use in accelerators. First, the memory requirements of this technique are significant, since the derivative information for the 6D coordinates of each particle must be stored for each simulation step simultaneously. This poses difficulties towards applying this technique to modeling collective effects such as wakefields or particle-particle interactions, both which significantly increase the number of computations for tracking the distribution through a given beamline. The use of high performance GPUs for particle tracking simulations (as is done here) and differentiable surrogate modeling techniques [36] could be used to surpass these limitations. Second, snapshot ensembling provides a simple heuristic for uncertainty estimation, but it is not well-calibrated to observed experimental uncertainties, as seen in the experimental case at AWA. Incorporating a more robust sta-

tistical interpretation using for example, Bayesian neural networks [40] in the future, will lead to better calibration. Finally, this method relies on the availability of differentiable physics models for accelerator elements. While the accelerator community is taking steps toward supporting fully differentiable particle tracking codes [41] and there is great interest in this for end-to-end simulation and physics analysis more broadly [42], at present no major particle tracking codes support it. It will take community effort to expand the advantages provided by this development for a wider set of beam manipulations.

ACKNOWLEDGMENTS

The authors would like to thank Lukas Heinrich and Michael Kagan for useful discussion during the early conceptual development of this work. This work was supported by the U.S. Department of Energy, under DOE Contract No. DE-AC02-76SF00515, the Office of Science, Office of Basic Energy Sciences and the Center for Bright Beams, NSF award PHY-1549132. This research used resources of the National Energy Research Scientific Computing Center (NERSC), a U.S. Department of Energy Office of Science User Facility located at Lawrence Berkeley National Laboratory, operated under Contract No. DE-AC02-05CH11231 using NERSC award ERCAP0020725.

Author Contributions: R.R. and A.E. conceived of the idea to combine differentiable simulations with machine learning for phase space tomography. R.R. led the studies and performed the work for phase space reconstruction.

A.E. and D.R. provided technical guidance and feedback. J.P.G. developed the differentiable simulation with guidance from R.R. and C.M. S.K., E.W. and J.P. assisted with experimental studies at AWA. R.R. and A.E. wrote

the manuscript. J.P.G., C.M. provided substantial edits to the manuscript. All authors provided feedback on the manuscript.

-
- [1] S. Nagaitsev, Z. Huang, J. Power, J. L. Vay, P. Piot, L. Spentzouris, J. Rosenzweig, Y. Cai, S. Cousineau, M. Conde, M. Hogan, A. Valishev, M. Minty, T. Zolkin, X. Huang, V. Shiltsev, J. Seeman, J. Byrd, Y. Hao, B. Dunham, B. Carlsten, A. Seryi, and R. Patterson, Accelerator and beam physics research goals and opportunities (2021).
- [2] P. Emma, R. Akre, J. Arthur, R. Bionta, C. Bostedt, J. Bozek, A. Brachmann, P. Bucksbaum, R. Coffee, F. J. Decker, Y. Ding, D. Dowell, S. Edstrom, A. Fisher, J. Frisch, S. Gilevich, J. Hastings, G. Hays, P. Hering, Z. Huang, R. Iverson, H. Loos, M. Messerschmidt, A. Miahnahri, S. Moeller, H. D. Nuhn, G. Pile, D. Ratner, J. Rzepiela, D. Schultz, T. Smith, P. Stefan, H. Tompkins, J. Turner, J. Welch, W. White, J. Wu, G. Yocky, and J. Galayda, First lasing and operation of an \angstrom-wavelength free-electron laser, *Nature Photonics* **4**, 641 (2010), publisher: Nature Publishing Group.
- [3] H. Li, Y. Sun, J. Vila-Comamala, T. Sato, S. Song, P. Sun, M. H. Seaberg, N. Wang, J. B. Hastings, M. Dunne, P. Fuoss, C. David, M. Sutton, and D. Zhu, Generation of highly mutually coherent hard-x-ray pulse pairs with an amplitude-splitting delay line, *Phys. Rev. Research* **3**, 043050 (2021).
- [4] Y. Sun, M. Dunne, P. Fuoss, A. Robert, D. Zhu, T. Osaka, M. Yabashi, and M. Sutton, Realizing split-pulse x-ray photon correlation spectroscopy to measure ultrafast dynamics in complex matter, *Phys. Rev. Research* **2**, 023099 (2020).
- [5] A. Marinelli, D. Ratner, A. A. Lutman, J. Turner, J. Welch, F. J. Decker, H. Loos, C. Behrens, S. Gilevich, A. A. Miahnahri, S. Vetter, T. J. Maxwell, Y. Ding, R. Coffee, S. Wakatsuki, and Z. Huang, High-intensity double-pulse x-ray free-electron laser, *Nature Communications* **6**, 10.1038/ncomms7369 (2015).
- [6] F.-J. Decker, K. L. Bane, W. Colocho, S. Gilevich, A. Marinelli, J. C. Sheppard, J. L. Turner, J. J. Turner, S. L. Vetter, A. Halavanau, C. Pellegrini, and A. A. Lutman, Tunable x-ray free electron laser multipulses with nanosecond separation, *Scientific Reports* **12**, 10.1038/s41598-022-06754-y (2022).
- [7] *Advanced Accelerator Development Strategy Report: DOE Advanced Accelerator Concepts Research Roadmap Workshop*, Tech. Rep. (USDOE Office of Science, Washington, DC (United States), 2016).
- [8] G. Ha, M. Cho, W. Gai, K.-J. Kim, W. Namkung, and J. Power, Perturbation-minimized triangular bunch for high-transformer ratio using a double dogleg emittance exchange beam line, *Physical Review Accelerators and Beams* **19**, 121301 (2016).
- [9] P. Piot, Y.-E. Sun, J. G. Power, and M. Rihaoui, Generation of relativistic electron bunches with arbitrary current distribution via transverse-to-longitudinal phase space exchange, *Physical Review Special Topics - Accelerators and Beams* **14**, 022801 (2011).
- [10] R. J. England, J. B. Rosenzweig, G. Andonian, P. Musumeci, G. Travish, and R. Yoder, Sextupole correction of the longitudinal transport of relativistic beams in dispersionless translating sections, *Physical Review Special Topics - Accelerators and Beams* **8**, 012801 (2005).
- [11] C. McKee, P. O'Shea, and J. Madey, Phase space tomography of relativistic electron beams, *Nuclear Instruments and Methods in Physics Research Section A: Accelerators, Spectrometers, Detectors and Associated Equipment* **358**, 264 (1995).
- [12] S. Hancock, M. Lindroos, E. McIntosh, and M. Metcalf, Tomographic measurements of longitudinal phase space density, *Computer Physics Communications* **118**, 61 (1999).
- [13] D. Stratakis, R. A. Kishek, I. Haber, M. Walter, R. B. Fiorito, S. Bernal, J. Thangaraj, K. Tian, C. Papadopoulos, M. Reiser, and P. G. O'Shea, Phase space tomography of beams with extreme space charge, in *2007 IEEE Particle Accelerator Conference (PAC)* (2007) pp. 2025–2029.
- [14] V. Yakimenko, M. Babzien, I. Ben-Zvi, R. Malone, and X.-J. Wang, Electron beam phase-space measurement using a high-precision tomography technique, *Physical Review Special Topics - Accelerators and Beams* **6**, 122801 (2003).
- [15] M. Röhrs, C. Gerth, H. Schlarb, B. Schmidt, and P. Schmüser, Time-resolved electron beam phase space tomography at a soft x-ray free-electron laser, *Physical Review Special Topics - Accelerators and Beams* **12**, 050704 (2009).
- [16] M. Gordon, W. Li, M. Andorf, A. Bartnik, C. Duncan, M. Kaemingk, C. Pennington, I. Bazarov, Y.-K. Kim, and J. Maxson, Four-dimensional emittance measurements of ultrafast electron diffraction optics corrected up to sextupole order, *Physical Review Accelerators and Beams* **25**, 084001 (2022).
- [17] E. Prat and M. Aiba, Four-dimensional transverse beam matrix measurement using the multiple-quadrupole scan technique, *Physical Review Special Topics - Accelerators and Beams* **17**, 052801 (2014).
- [18] A. Green and Y.-M. Shin, Implementation of Quadrupole-scan Emittance Measurement at Fermilab's Advanced Superconducting Test Accelerator (ASTA), in *6th International Particle Accelerator Conference* (2015) p. MOPMA052.
- [19] A. Mostacci, M. Bellaveglia, E. Chiadroni, A. Cianchi, M. Ferrario, D. Filippetto, G. Gatti, and C. Ronsivalle, Chromatic effects in quadrupole scan emittance measurements, *Phys. Rev. ST Accel. Beams* **15**, 082802 (2012).
- [20] S. Webb, *The Physics of Medical Imaging* (CRC Press, Boca Raton, 1987).
- [21] A. C. Kak and M. Slaney, *Principles of computerized tomographic imaging* (SIAM, 2001).

- [22] K. M. Hock and M. G. Ibison, A study of the maximum entropy technique for phase space tomography, *Journal of Instrumentation* **8** (02), P02003.
- [23] K. Hock and A. Wolski, Tomographic reconstruction of the full 4d transverse phase space, *Nuclear Instruments and Methods in Physics Research Section A: Accelerators, Spectrometers, Detectors and Associated Equipment* **726**, 8 (2013).
- [24] J. C. Wong, A. Shishlo, A. Aleksandrov, Y. Liu, and C. Long, 4D transverse phase space tomography of an operational hydrogen ion beam via noninvasive 2D measurements using laser wires, *Physical Review Accelerators and Beams* **25**, 042801 (2022).
- [25] M. Wang, Z. Wang, D. Wang, W. Liu, B. Wang, M. Wang, M. Qiu, X. Guan, X. Wang, W. Huang, and S. Zheng, Four-dimensional phase space measurement using multiple two-dimensional profiles, *Nuclear Instruments and Methods in Physics Research Section A: Accelerators, Spectrometers, Detectors and Associated Equipment* **943**, 162438 (2019).
- [26] B. Hermann, V. A. Guzenko, O. R. Hürzeler, A. Kirchner, G. L. Orlandi, E. Prat, and R. Ischebeck, Electron beam transverse phase space tomography using nanofabricated wire scanners with submicrometer resolution, *Physical Review Accelerators and Beams* **24**, 022802 (2021).
- [27] D. Sagan, Bmad: A relativistic charged particle simulation library, *Computational accelerator physics. Proceedings, 8th International Conference, ICAP 2004, St. Petersburg, Russia, June 29-July 2, 2004*, Nucl. Instrum. Meth. **A558**, 356 (2006), proceedings of the 8th International Computational Accelerator Physics Conference.
- [28] J. Lawson, R. Gluckstern, and P. M. Lapostolle, Emission, entropy and information, *Part. Accel.* **5**, 61 (1973).
- [29] D. P. Kingma and J. Ba, Adam: A Method for Stochastic Optimization, arXiv:1412.6980 [cs] (2017), arXiv:1412.6980.
- [30] Y. A. LeCun, L. Bottou, G. B. Orr, and K.-R. Müller, Efficient BackProp, in *Neural Networks: Tricks of the Trade: Second Edition*, Lecture Notes in Computer Science, edited by G. Montavon, G. B. Orr, and K.-R. Müller (Springer, Berlin, Heidelberg, 2012) pp. 9–48.
- [31] A. Paszke, S. Gross, F. Massa, A. Lerer, J. Bradbury, G. Chanan, T. Killeen, Z. Lin, N. Gimelshein, L. Antiga, A. Desmaison, A. Kopf, E. Yang, Z. DeVito, M. Raison, A. Tejani, S. Chilamkurthy, B. Steiner, L. Fang, J. Bai, and S. Chintala, PyTorch: An Imperative Style, High-Performance Deep Learning Library, in *Advances in Neural Information Processing Systems 32*, edited by H. Wallach, H. Larochelle, A. Beygelzimer, F. d. Alché-Buc, E. Fox, and R. Garnett (Curran Associates, Inc., 2019) pp. 8024–8035.
- [32] M. Rosenblatt, Remarks on some nonparametric estimates of a density function, *The annals of mathematical statistics*, 832 (1956).
- [33] G. Huang, Y. Li, G. Pleiss, Z. Liu, J. E. Hopcroft, and K. Q. Weinberger, Snapshot ensembles: Train 1, get m for free, arXiv preprint arXiv:1704.00109 (2017).
- [34] M. Conde, S. Antipov, D. Doran, W. Gai, Q. Gao, G. Ha, C. Jing, W. Liu, N. Neveu, J. Power, *et al.*, Research program and recent results at the argonne wakefield accelerator facility (awa), *Proc. IPAC'17*, 2885 (2017).
- [35] L. Zheng, J. Shao, Y. Du, J. G. Power, E. E. Wisniewski, W. Liu, C. E. Whiteford, M. Conde, S. Doran, C. Jing, C. Tang, and W. Gai, Experimental demonstration of the correction of coupled-transverse-dynamics aberration in an rf photoinjector, *Physical Review Accelerators and Beams* **22**, 072805 (2019), publisher: American Physical Society.
- [36] A. Edelen and C. Mayes, Neural Network Solver for Coherent Synchrotron Radiation Wakefield Calculations in Accelerator-based Charged Particle Beams (2022), arXiv:2203.07542 [physics].
- [37] J. Qiang, Differentiable self-consistent space-charge simulation for accelerator design, arXiv preprint arXiv:2207.07997 (2022).
- [38] R. Roussel, G. Andonian, J. Rosenzweig, and S. Baturin, Longitudinal current profile reconstruction from a wakefield response in plasmas and structures, *Physical Review Accelerators and Beams* **23**, 121303 (2020), publisher: American Physical Society.
- [39] R. Roussel, A. Edelen, D. Ratner, K. Dubey, J. Gonzalez-Aguilera, Y. Kim, and N. Kuklev, Differentiable Preisach Modeling for Characterization and Optimization of Particle Accelerator Systems with Hysteresis, *Physical Review Letters* **128**, 204801 (2022), publisher: American Physical Society.
- [40] L. V. Jospin, H. Laga, F. Boussaid, W. Buntine, and M. Bennamoun, Hands-on bayesian neural networks—a tutorial for deep learning users, *IEEE Computational Intelligence Magazine* **17**, 29 (2022).
- [41] S. Biedron, L. Brouwer, D. Bruhwiler, N. Cook, A. Edelen, D. Filippetto, C.-K. Huang, A. Huebl, N. Kuklev, R. Lehe, *et al.*, Snowmass21 accelerator modeling community white paper, arXiv preprint arXiv:2203.08335 (2022).
- [42] T. Dorigo, A. Giammanco, P. Vischia, M. Aehle, M. Bawaj, A. Boldyrev, P. d. C. Manzano, D. Derkach, J. Donini, A. Edelen, *et al.*, Toward the end-to-end optimization of particle physics instruments with differentiable programming: a white paper, arXiv preprint arXiv:2203.13818 (2022).